Numerical damage models in biological tissues using a structural approach

Pierre-Jean Arnoux, Jean Bonnoit, Patrick Chabrand, Michel Jean, Martine Pithioux

Numerical damage models using a structural approach: application in bones and ligaments

P.J. Arnoux[1,2], J. Bonnoit[2], P. Chabrand[1], M. Jean[1], and M. Pithioux[1,a]

[1] Laboratoire de Mécanique et d'Acoustique, CNRS, équipe MMCB, 31 chemin J. Aiguier, 13402 Marseille, France
[2] Laboratoire de Biomécanique Appliquée, INRETS, Faculté de Médecine, boulevard P. Dramard, 13916 Marseille, France

Abstract. The purpose of the present study was to apply knowledge of structural properties to perform numerical simulations with models of bones and knee ligaments exposed to dynamic tensile loading leading to tissue damage. Compact bones and knee ligaments exhibit the same geometrical pattern in their different levels of structural hierarchy from the tropocollagen molecule to the fibre. Nevertheless, their mechanical behaviours differ considerably at the fibril level. These differences are due to the contribution of the joints in the microfibril-fibril-fibre assembly and to the mechanical properties of the structural components. Two finite element models of the fibrous bone and ligament structure were used to describe damage in terms of elastoplastic laws or joint decohesion processes.

1 Introduction

The aim of this work was to develop a specific model to study failure of fibrous structures submitted to dynamic loading. Our goal was to describe the failure of such materials subsequent to loss of cohesion between fibres, assumed to be the structural element most susceptible to failure. This assumption implies that failure in these kinds of structures does not occur by rupture of the fibres themselves but rather as a consequence of an avalanche process by rupture of the joints. An appropriate model would thus have to consider both longitudinal and transverse joints between fibres. We developed a multi-scale method to deal with the various levels of the structural hierarchy. The purpose of this study was to determine how numerical experiments performed on a rough model of the cohesive composite material comprising elastic fibres may help understand the brittle or ductile behaviour of these tissues when they were subjected to dynamic tensile loading. This approach was based on two different finite element models of fibrous material. An elastic model with perfect-elastoplastic elements was used to describe the connections between the fibres constituting the model. Damage was introduced in the form of perfect plastic flows of the rod elements forming the joints between fibres. A second elastic model with unilateral constraints and friction contact was used to describe the joints between the fibres constituting the model [1,2]. Damage was described by fibres decohesion mechanisms.

Fibrous materials found in nature include many biological tissues such as bones and ligaments. The mechanical properties of these materials, and more particularly their failure behaviour, is of interest in many domains. Specific applications include care for victims of accidents or sports trauma. Cortical bones and ligaments of the knee were subjected to shocks leading to tears, injury and failure. Certain authors [3] have used a homogeneous micro-macro model. Others have described the constitutive equations using a thermodynamic approach [4,5], or a phenomenological approach [6–12]. The structural approach [13–17] is based on knowledge of the tissue microstructure. These models have proven to be inadequate to study failure of these materials and while exploration of hard and soft tissues is a highly developed field of research, the mechanical behaviour of these tissues exposed to dynamic loading causing damage and failure has not drawn the attention of many authors. Damage models, the main models presented in the literature [18], have been based on fibre-ligament or fibre-bone assemblies. These discrete models deal with an assembly of disjointed fibres with stochastically distributed lengths where failure is described in terms of the strain level in each fibre. They have performed well under quasi-static conditions. In our work, we show that bones and ligaments exhibit a structural hierarchy. We therefore developed two models using a structural approach that requires, in this context, a multi-scale

[a] e-mail: pithioux@lma.cnrs-mrs.fr

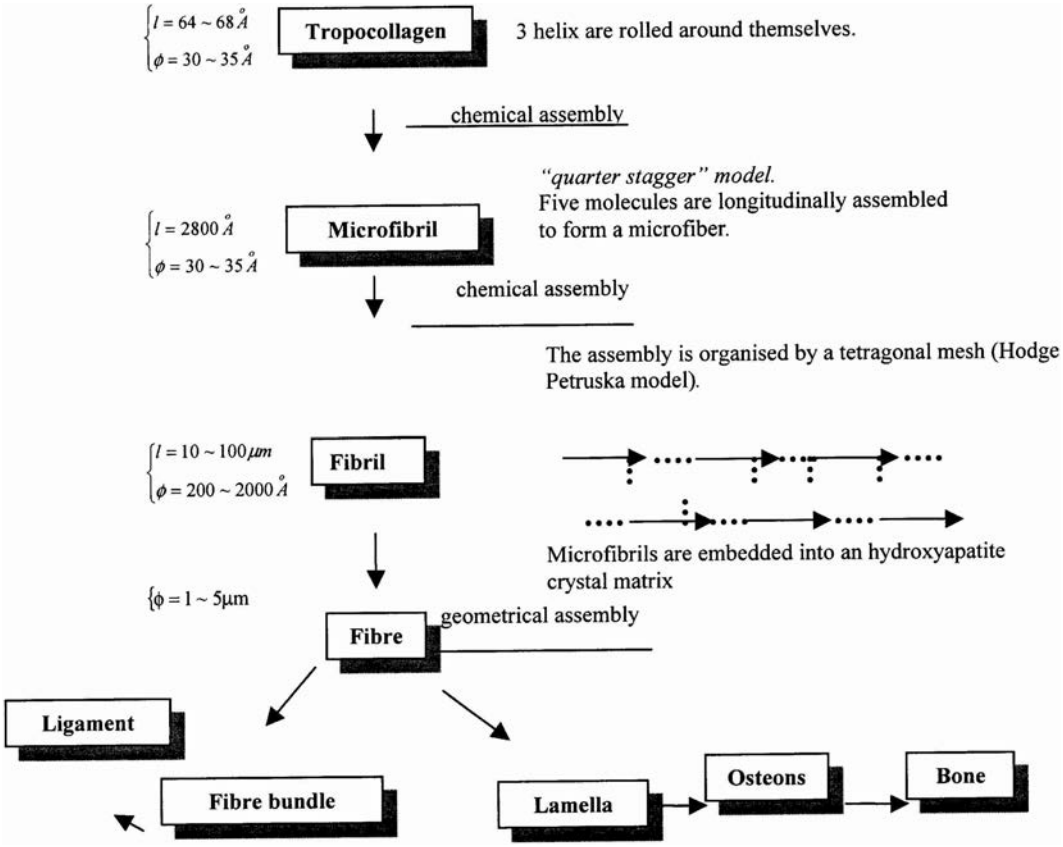

Fig. 1. Assembly of the different hierarchical levels in the ligament and bone structure. The geometric similarities between ligaments and bone were based on the microfibril fibre assembly. l represents the length and ϕ the diameter of the structure considered.

method. These models were used to simulate tensile experiments where the fibrous structure was exposed to dynamic stress.

2 Structural analysis of bones and ligaments

In order to understand the rationale for defining such a fibrous model, it is useful to review the general properties of the structural hierarchy composing biological tissues.

Ligaments and bones are highly complex structures [19–21] which can be viewed as composite materials composed of various constituents in a geometrical assembly. Compact bones and knee ligaments exhibit the same geometrical pattern in their different levels of structural hierarchy from the tropocollagen molecule to the fibre (Fig. 1). However, although the same mechanical properties are observed in ligaments and bones up to the microfibril level [16,17], important differences are observed from the fibril level up to the macroscopic level (*i.e.* ligaments exhibit viscoelastic properties and bones exhibit elastoplastic properties). Therefore in order to understand the mechanical properties of the material as a whole, it is essential to examine the contribution of each level of the structural hierarchy. The main deformation mechanisms can occur at four different levels.

The lowest level is the tropocollagen molecule composing the microfibril. Measuring 2800 Å in length, the tropocollagen molecule has elongation properties which set its molecular profile [16,17,22–24]. Mechanical models based on the waviness of the microfibrils have been proposed [25,26]. At this level, the microfibrils were found to be elastic [14,27].

The Hodge Petruska model [16,17,28] has been used to describe the second level. The arrangement at this scale (fibril length = 10 mm to 100 mm) shows regions of overlapping fibrils and gaps with different mechanical behaviours for ligaments and bones, essentially because of the nature of their joint components. In bone structure, joints are made of a mineral, hydroxyapatite, while in ligament structure joints have an organic configuration without a mineral component. Observed experimental behaviours [16,17,29,30] have shown that ligaments can be described as a viscoelastic solid and bone as an elastoplastic solid.

- The fiber, the third level, is a geometrical assembly of disjointed fibrils embedded in an amorphous substance. Loading applies pressure to fibres causing fluid to exude from the tissue, so the material exhibits a viscous behaviour [31,32].
- The fourth level is the fibre-ligament or fibre-bone assembly, which cannot be precisely described in terms

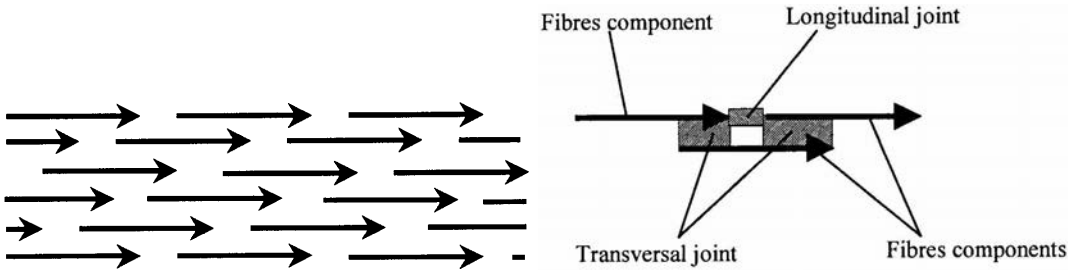

(a) (b)

Fig. 2. (a) Fibrous assembly. (b) Example of unit fibrous assembly projection onto a two dimensional plane.

of fibre interactions. In addition, the amorphous substance can be described as an incompressible fluid.

3 The fibrous model

The biological materials studied are structured on different scales, from the collagenous elementary constitutive molecules (tropocollagen) to microfibrils, fibrils, fibres and finally bundles of fibres. Although collagen fiber debonding and pullout represent important failure mechanism in failure of bones and ligaments, cracking and plastic deformation of the ground substance are equally or more important contributor to behaviour. It might therefore be conjectured that, due to the fibrous structure of this biological material, the failure process might be caused by successive decohesion events occurring at different scales and aggregating so as to generate micro-voids or microcracks, the aggregates themselves generating larger scale voids or cracks. There remains the possibility of exploring assemblies of model-fibres linked together with appropriately distributed cohesive forces. Given the fibrous structure of the model, the ability to bear tensile stress is due to two classes of cohesive forces: forces exerted by the fore end of fibres on the aft end of the previous fibre (head to tail or longitudinal cohesive force); forces exerted from flank to flank between neighbouring fibres (flank to flank or transverse cohesive force). In this study, tensile loading was considered in the longitudinal axis of the fibres. The head to tail forces were mainly tensile forces, while the flank to flank forces were mainly shear forces. The constitutive laws were therefore developed using a fibrous model subjected to tensile traction applied in the direction of the fibre axis (this model could be a fibril). The material was assumed to be homogeneous and regular. Because of the dynamic kinematics involved, damage was assumed to be preponderant and viscosity was neglected. The following fibrous model (*cf.* Fig. 2a) consists of an assembly of fibres (which could be microfibrils, fibrils and fibres), in which joints are formed laterally and longitudinally between the fibres (*cf.* Figs. 2a and 2b).

3.1 Elastoplastic description of the joints

One way of describing damage in joints is to model a joint as a perfect elastoplastic material. For the mechanical properties, the fibres were assumed to be elastic and the joints to be elastoplastic. The constitutive laws in the joints were defined by equations (1, 2):

$$\text{where } \sigma = E\varepsilon \text{ when } \varepsilon \leq \varepsilon_{\text{rup}} \tag{1}$$

$$\text{and } \sigma = \sigma_{\text{rup}} \text{ when } \varepsilon \succ \varepsilon_{\text{rup}} \tag{2}$$

with, σ and ε the stress and strain in the joints, σ_{rup} and ε_{rup} the failure stress and strain of the joints.

3.2 The cohesive model

In this model, the interactions between fibres were described using unilateral constraint and frictional cohesive contact laws.

By considering q_{N} the normal displacement from one fibre to another and $R = (R_{\text{T}}, R_{\text{N}})$ the reaction force (for which R_{T} and R_{N} are respectively the tangential and normal reaction forces between the two fibres in a local coordinate system) the unilateral constraint defined by Signorini is written as follow (3):

$$q_{\text{N}} \geq 0,\ R_{\text{N}} + l \geq 0,\ (q_{\text{N}}, R_{\text{N}} + l) = 0 \tag{3}$$

where l is the longitudinal cohesive threshold.

The joint model was given by a cohesive Mohr Coulomb law between nodes candidates for contact (*cf.* Fig. 3a) which corresponds to a vertical displacement of the Coulomb cone. With such a cohesive law between fibres, three main situations are possible at the joints; (i) the fibres stick together inside the cone (A for instance in Fig. 3a), (ii) stickness is lost on the cone border (C for instance in Fig. 3a), and friction, corresponding to damage, occurs between the fibres, (*i.e.* the joints break between the fibre components), (iii) no contact is possible between fibres (contact is lost). With the Mohr Coulomb law, the formulation for the adhesive unilateral constraint becomes (4):

$$q_{\text{N}} \geq 0;\ R_{\text{N}} \geq -l;\ q_{\text{N}} \cdot (R_{\text{N}} + l) = 0. \tag{4}$$

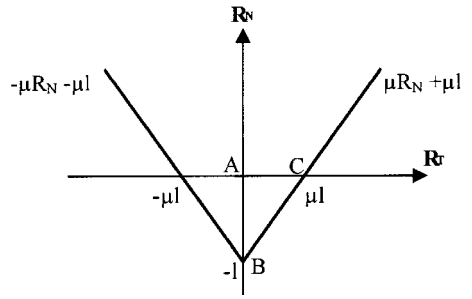

(a)

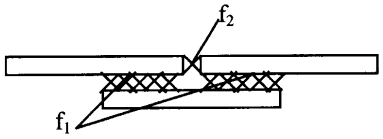

(b)

Fig. 3. (a) Mohr Coulomb cohesive law. (b) f_1 is the cohesive coefficient of the shear between two fibres layers. f_2 is the tensile cohesive coefficient for the fibre cohesion on the same layer.

Fig. 4. Boundary conditions of the problem. On side AD, the displacements were fixed. On side BC, 5 m/s velocities were applied.

The corresponding sliding law with adhesion defined by the threshold μl is given in relations (4a, 4b and 4c):

$$U_{\mathrm{T}} = 0 \Rightarrow R_{\mathrm{T}} \in]-\mu R_{\mathrm{N}} - \mu l;\ \mu R_{\mathrm{N}} + \mu l[\quad (4a)$$

$$U_{\mathrm{T}} < 0 \Rightarrow R_{\mathrm{T}} = -\mu R_{\mathrm{N}} - \mu l \quad (4b)$$

$$U_{\mathrm{T}} > 0 \Rightarrow R_{\mathrm{T}} = \mu R_{\mathrm{N}} + \mu l. \quad (4c)$$

The static sliding coefficient μ_{s} is defined by $\mu_{\mathrm{s}} = \mathrm{tg}\,\alpha = f_2/f_1$ (*cf.* Fig. 3a).

The cohesive thresholds differ between longitudinal (f_1) and transverse (f_2) joints and are related to maximal head to tail and flank to flank cohesive forces (Fig. 3b). With this model, damage results from fibre decohesion mechanisms which occur at around 5% of strain levels in the case of bone, and 25% of strain levels in that of ligaments. One way of introducing heterogeneity into the material is to randomise failure thresholds.

4 The finite element models

In a finite element model, a representative volume is an assembly of 21 fibres arranged longitudinally in 30 successive layers. To study the influence of the geometry on the results, we also simulated a structure composed of 7 fibres longitudinally arranged in 90 successive layers and 42 fibres longitudinally arranged in 60 successive layers. As boundary conditions on the lateral sides, the displacements were taken to be zero in the case of all left hand side nodes ($Ux = 0$) and velocities of 5 m/s were applied to all right hand side nodes (*cf.* Fig. 4). A periodicity boundary condition may be viewed as that showing the best fit to the influence of material surrounding the sample in a tensile experiment. For this, on the upper and lower sides, we chose to set stress σ_{22} to 0 with the displacement of the upper and lower sides being the same. The same mesh, corresponding to a two dimensional tetragonal assembly, was used for ligaments and bones (because of the geometric similarities).

The two different finite element modelling methods used to deal with this problem are presented in the following section.

4.1 Elastoplastic model

In the elastoplastic model, the assembly was performed using rod elements to simulate fibres and joints. Each fibre and longitudinal joint (in the case of head to tail forces) was obtained using a single rod element. Transverse joints (flank to flank forces) were obtained using cross rods. In order to improve the sensitivity of the mesh, transverse joints could be made using one or several cross rods (*cf.* Figs. 5a and 5b). In this latter case, the number of cross rods depended on the overlap and gap regions present in the fibrous assembly (*cf.* Figs. 2a and 2b). In the case of a single cross rod (21 fibres arranged longitudinally in 30 successive layers), the mesh obtained consisted of 3780 nodes, 6128 elements measuring 6.682 μm in length. In the second case (several cross-rods) the mesh consisted of 6300 nodes, 15896 elements measuring 6.682 μm in length.

Several computations were performed with the ABAQUS software, in which a Newton implicit method was used. Each load case was performed in dynamic conditions (velocity equals 5 m/s). Randomised Young's modulus of the fibres, mineral and ultimate stress of joints at failure were tested.

4.2 Cohesive model

With the cohesive model, each fibre was simulated by 2D brick elements consisting of eight T3-triangles. In the case of bone, the bricks were designed to describe the mineral and collagen components as a single equivalent material. In the case of ligament, bricks represented only collagen. The dynamic problem was solved using LMGC software based on the Non Smooth Contact Dynamics method [1,2].

(a) (b)

Fig. 5. (a) Transverse joint with one cross-rod. (b) Transverse joint using several cross-rods.

5 Application to biological materials

We tested these models using biological data published in the literature. Several authors [6,12,14,16,17,29,33] have studied mechanical properties (Young's modulus, Poisson ratio and density) of collagen and hydroxyapatite and values used in our numerical simulation were determined from their work. In the case of bones, values of failure thresholds are taken within the plasticity values of mineral hydroxyapatite. In the case of ligaments, weakness values were used for thresholds. The representative volume was an assembly of 21 fibres longitudinally arranged in 30 successive layers which corresponds to the length of one fibril.

5.1 Elastoplastic model

It must be noted that mechanical properties of transverse joints (consisting of one or several cross rods) were calculated in order to have the same properties whatever the number of cross rods used for the joints. Young's modulus, Poisson ratio and density of ligaments and bone fibres were 0.8 GPa and 9 GPa, 0.3 and 0.35, and 1.2×10^3 kg/m^3 and 1.3×10^3 kg/m^3 respectively. In both structures, the joints were taken to be stiffer than the fibrous elements in view of Sasaki's experimental results [16,17]. The mechanical properties of joints for ligaments and the bones were obtained using Young's modulus, Poisson ratio and the ultimate stress at joint failure (plasticity yield). Young's modulus was taken to be between 0.8 GPa and 2 GPa for ligaments, and between 80 and 150 GPa for bones (hydroxyapatite). Poisson ratio was between 0.28 and 0.3 in both cases [33–35]. The ultimate stress was between 50 MPa and 100 MPa for ligaments, and between 120 MPa and 200 MPa for bones. Joint density was 1.2×10^3 kg/m^3 for ligaments and 2×10^3 kg/m^3 for bones.

5.2 Cohesive model

Ligaments and bones fibres were assumed to be elastic with a Young's modulus taken between $E = 0.6$ GPa and 1.2 GPa for ligaments and between $E = 11$ GPa and 16 GPa for bones. Young's modulus was taken as an average of Young's modulus for collagen and hydroxyapatite because the bricks described the mineral and collagen components as a single equivalent material. In both cases the density was $d = 1.2 \times 10^3$ kg/m^3 for ligaments and 2×10^3 kg/m^3 for bones; Poisson ratio was $\nu = 0.33$.

6 Results

6.1 The elastoplastic model

In both structures, von Mises stresses and plastic deformation curves showed that the most stressed joints were the longitudinal ones. Because of the dynamics, the deformation mechanisms acted like a traction wave which was reflected on the left hand side where zero displacements were prescribed. These effects may result in plastic deformations, as was observed in joints. Depending on the loads, boundary conditions, geometry or scattering of the mechanical properties, the von Mises stresses, the plastic deformation and the stress-strain curves showed several possible damage modes. The stress-strain curves show that the value of the failure force on the structure was the same whatever the dimension of the geometry [36].

First, a failure on the left and right hand side propagated vertically towards the two extremities of the structure and secondly, a sliding failure occurred in the structure combining appearance of quasi vertical cracks and debonding fibres. It can be seen from the stress displacement (Figs. 6a and 6b) that the results were in good agreement with the experimental data [8,12,14,36] and could be divided into two parts:

- first, an elastic linear region in which the Young's modulus values ranged around 0.5 GPa and 9 GPa for ligaments and bones;
- secondly, a damage region up to failure.

Figure 6a illustrates two types of behaviour that could be simulated using different types of boundaries. In the first case, the structure was isolated and the results showed a brittle behaviour (as in the case of compact bones and cruciate ligaments). In the second case, the sample was subjected to a periodic boundary, the behaviour of the structure in this case was ductile (as in the case of collateral ligaments). Figure 6b shows that introducing scattered mechanical properties into the material yielded at a variably earlier stage. This parameter would represent the porosity of the material. If the structure was assumed to be crystalline (with weak porosity) failure came later than if the structure was supposed to be heterogeneous (with important porosity).

6.2 The cohesive model

Qualitatively, the results obtained with the cohesive model were in good agreement with those obtained with the

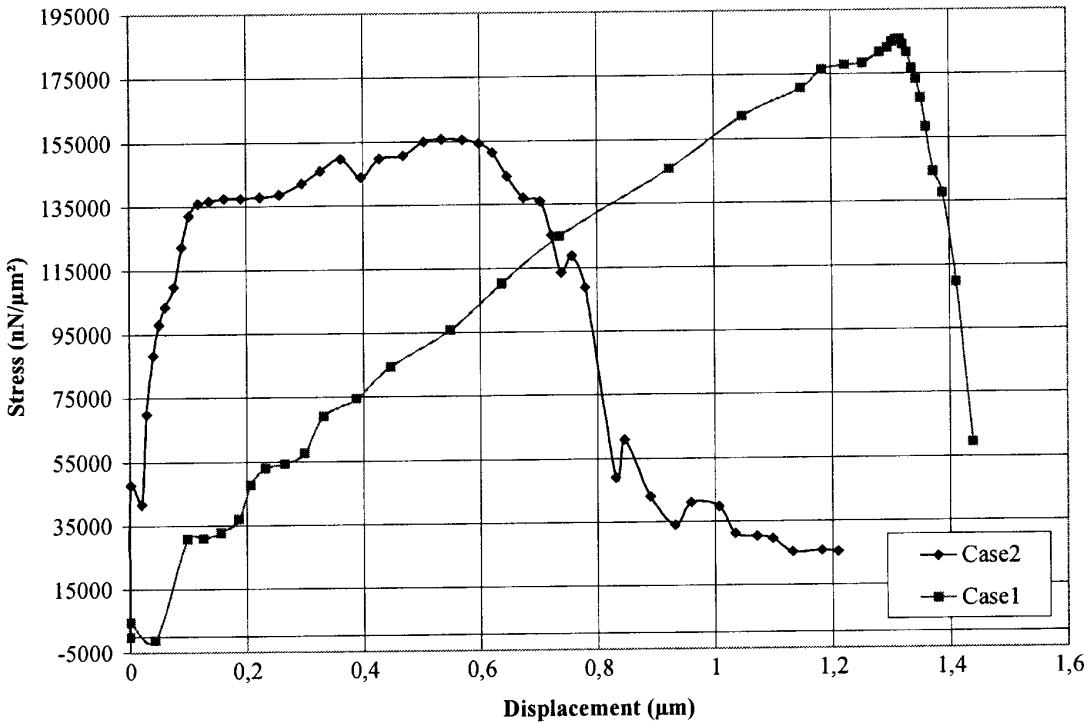

(a)

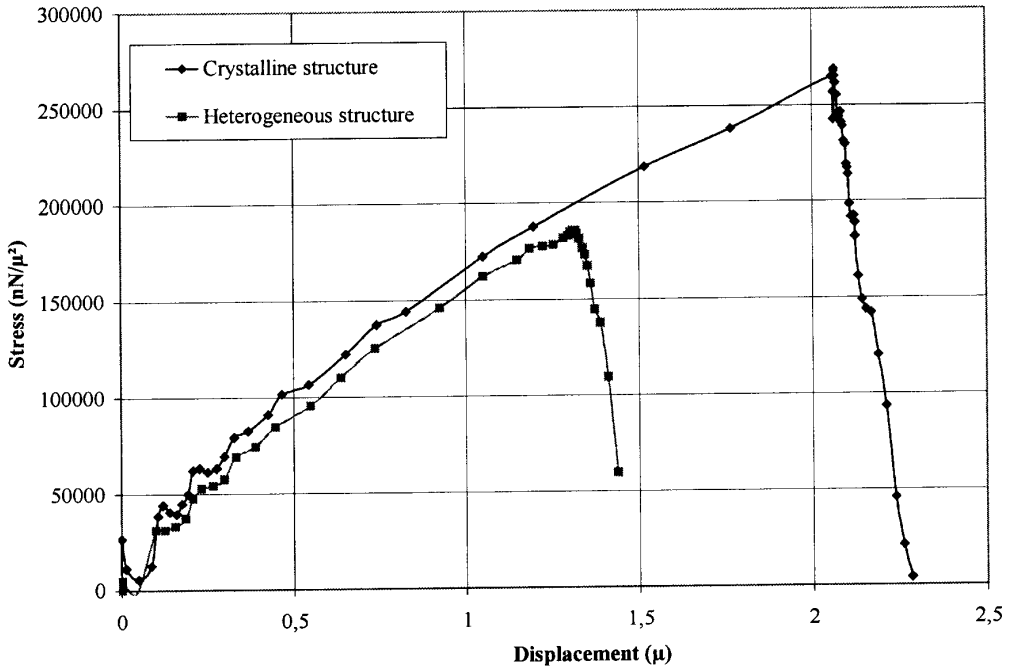

(b)

Fig. 6. (a) Effects of boundary conditions on the stress displacement curve, in the case of the bone or ligament structure. In case 1, the structure is assumed to be isolated whereas in case 2, the sample is subjected to periodic boundary conditions. (b) Effects of the scattering on the failure of the structure.

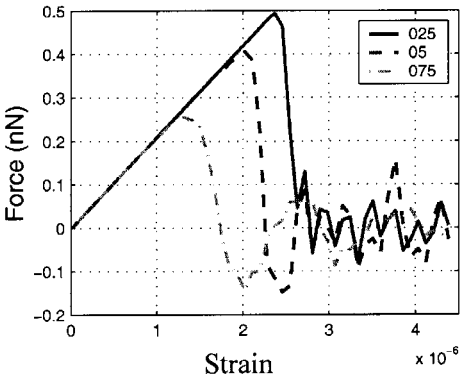

Fig. 7. Effects of the scattering on the force deformation curve. The scattering parameter was more important for 0.75 than for 0.5 and for 0.5 than for 0.25.

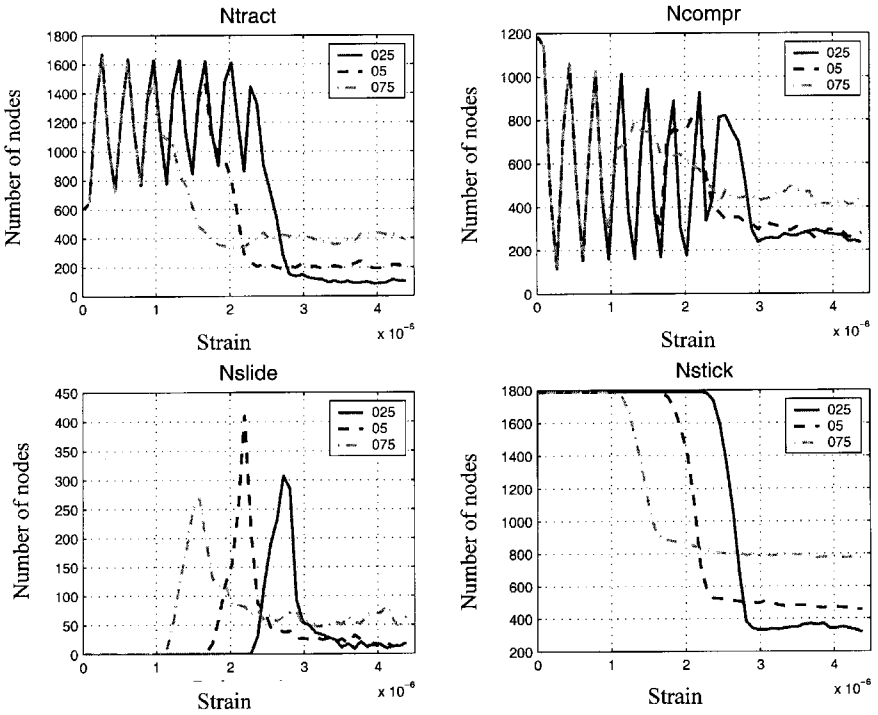

Fig. 8. Effects of the scattering on the evolution of the node status (Nodes under traction, Nodes under compression, sliding Nodes, sticking Nodes).

elastoplastic model. The stress-strain curve could be divided into a linear elastic portion and a damage portion up to the complete failure of the structure. As observed in the case of the elastoplastic model, the scattering parameters had a strong influence on the behaviour and on the failure profile (Fig. 7). The time course of the damage processes could be followed more closely by examining that of the node status (sticking, sliding, traction, compression, ...) (Fig. 8). Oscillations showed tensile-compressive wave propagation. This information appeared to be useful for determining the relevant parameters for a macroscopic failure model. Figures 9a, 9b, 9c illustrate a failure process. Failure occurred suddenly, comparable to an avalanche process. In this situation, the decohesion of a few joints triggered a step by step failure process in the neighbourhood. Longitudinally and transversally connected joints were also damaged and the structure was broken in only a few steps.

7 Discussion and conclusion

In these two models, bones and ligaments were described as fibrous structures in which deformation occurs in the fibrous elements and damage results from the failure of joints between the fibres. Two finite element models were used to describe the behaviour of this structure, based on two different methods of modelling joint behaviour. With each model we were able to establish how different parameters, mainly the scattering parameters, can strongly affect the description of the failure processes. The cohesive

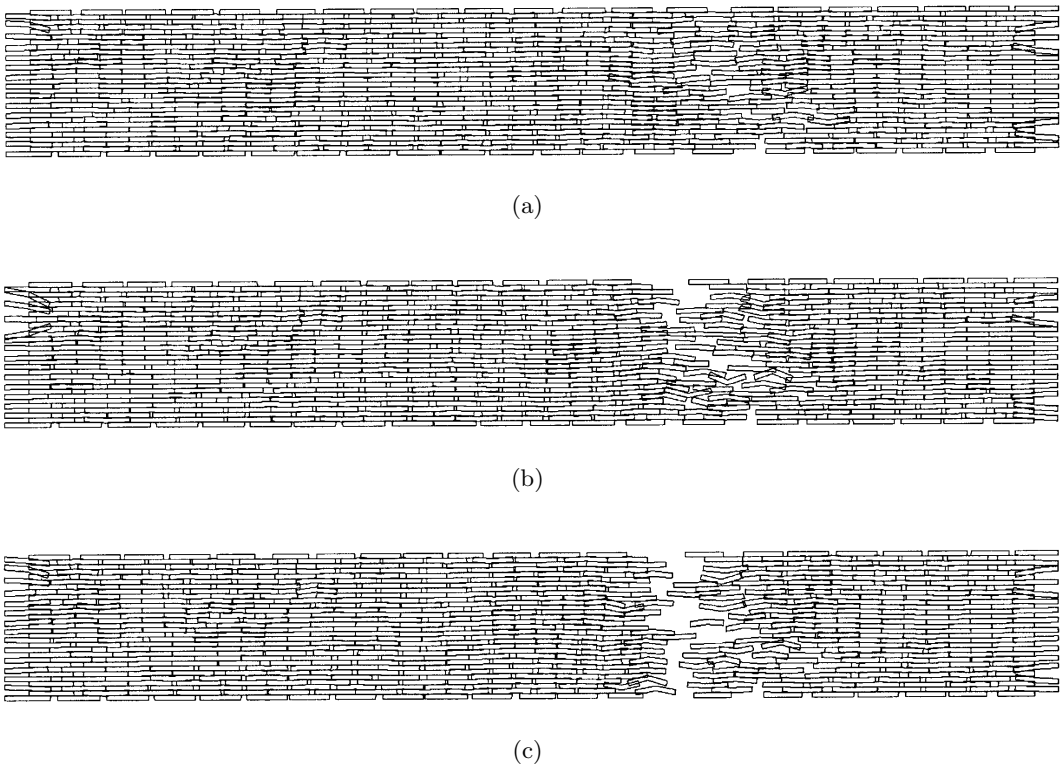

Fig. 9. (a) Displacement at $t = 0.013$ μs with 10^6 magnification. (b) Displacement at $t = 0.014$ μs with 10^6 magnification. (c) Displacement at $t = 0.015$ μs with 10^6 magnification.

model gave a physical description of the damage resulting from joint decohesion processes. Differences in failure stress between longitudinal and transverse joints (contact with the head and flank of a fibre) did not affect the behaviour of the structure, whereas scattering, and the friction coefficient after failure, could be used to control the behaviour and the course of damage in the model.

In these two finite element models, the viscosity of the structure was not taken into account so as to emphasise the decohesion process. Further calculations would be useful to introduce the viscous component.

The first model using ABAQUS is easy to apply. The analysis can be performed with readily available software implementing an elastoplastic perfect law. The second model based on cohesive laws provides a more accurate description of the phenomena in longitudinal and transverse joints.

This work was a first step towards describing a structural failure model in which damage occurs as the result of decohesion between the longitudinal and transverse joints. These models were helpful in understanding failure mechanisms and the parameters which influence failure in fibrous structures. These parameters are pertinent to study failure in the microstructure and therefore in the macrostructure.

To study ligaments using a combined microscopic/macroscopic assembly, more information yet to be obtained experimentally, would be needed to describe the assembly. By making a certain number of assumptions to simplify the description of the structure, we were able to propose several ways to model the microscopic/macroscopic assembly. First, to obtain a homogeneous model, we assumed the fibril model to be a representative elementary volume of the ligament. In this way, all the fibres in the fibre bundles are assumed to lie in the same direction so that, after applying a scaling factor, the microscopic failure behaviour depicts the macroscopic failure behaviour. The second way is to construct the fibril/fibre assembly with the fibril as the basic component of the fibre. In this multi-scale method, the structure is composed of elementary fibril structures whose behaviour is that observed for the fibrils. The ligament can then be described as an assembly of disjointed fibres. The final method is to introduce a viscous fluid between the fibres, and to take into consideration the orientation of the main fibre bundles in the ligament.

The bone model could be based on either a fibril, a fibre or a lamellar structure because all these hierarchical structures are oriented in the same direction. The microscopic/macroscopic assembly could be obtained in the same way as in the case of ligaments using a multiscale method. However, the lamellar structure of bone is constituted of fibres oriented horizontally, vertically and obliquely. Finally, the orientation of the fibres in the

lamellar structure must be analysed [37] to obtain the behaviour of the macrostructure of bone.

In these two finite element models, the qualitative results obtained were quite in line with those obtained at the macroscopic level reported in the literature.

In conclusion, we propose a new investigation in addition to those previously developed [18,38,39] for cortical bone and knee ligament modelling. For both structures modelled here, statistics on the failure mode giving the evolution of the node status could be used to obtain an overall microscopic/macroscopic scale assembly. Failure of these structures depends on the scattering parameter, the most important parameter in this model. The physical meaning of the scattering parameter is given by the porosity of the material. This approach enables a description of the internal value of the microscopic and therefore macroscopic phenomenological model dealing with the physics of damage processes.

References

1. M. Jean, *Frictional contact in rigid or deformable bodies: numerical simulation of geomaterials*, edited by A.P.S. Salvaduai, J.M. Boulon (Elsevier Science Publisher, Amsterdam), pp. 463–486.
2. M. Jean, Comput. Methods Appl. Mech. Eng. **177**, 235 (1999).
3. J.M. Crolet, B. Aoubiza, A. Meunier, J. Biomech. **26**, 677 (1993).
4. D.N. Bingham, P.H. DeHoff, J. Biomech. Eng. **101**, 15 (1979).
5. D.R. Carter, W.E. Caler, J. Orthopead. Res. **3**, 84 (1985).
6. W. Bonfield, C.H. Li, J. Appl. Phys. **37**, 869 (1966).
7. F.W. Cooke, H. Zeidman, S.J. Scheifele, J. Biomed. Mater. Res. Symp. **4**, 383 (1973).
8. A. Viidik, *Functional properties of collagenous tissues. International Review of Connective Tissue Research, VI* (Academic press, New York, 1973).
9. A. Viidik, *Mechanical properties of parallel-fibred collagenous tissues, Biology of collagen* (London: Academic press, 1980), pp. 237–255.
10. J.C. Barbenel, J.H. Evans, J.B. Finlay, *Stress-strain time relation for soft connective tissues. Perspectives in Biomedical Engineering*, edited by R.M. Kenedi (London Macmillan, 1973).
11. R. Sanjeevi, N. Somanathan, D. Ramaswamy, J. Biomech. **15**, 181 (1982).
12. Y.C. Fung, *Biomechanics. Mechanical properties of living tissues* (Springer-Verlag, 1993).
13. K. Piekarski, J. Appl. Phys. **41**, 215 (1970).
14. K. Piekarski, Int. J. Eng. Sci. **11**, 557 (1973).
15. W. Decreamer, M. Maes, V. Vanhuyse, P. Vanpeper-Strate, J. Biomech. **13**, 550 (1980).
16. N. Sasaki, S. Odajima, J. Biomech. **29**, 655 (1996).
17. N. Sasaki, S. Odajima, J. Biomech. **29**, 1131 (1996).
18. M. Kwan, S. Woo, J. Biomech. Eng. **111**, 361 (1989).
19. F.G. Evans, S. Bang, Am. J. Anat. **120**, 79 (1967).
20. J. Kastelic, A. Galeski, E. Bear, Connect. Tissue Res. **6**, 11 (1978).
21. S. Weiner, W. Traub, The Federation of American Societies for Experimental Biology Journal **6**, 879 (1992).
22. E. Bonucci, P.M. Motta, Collagen mineralization: Aspects of structural relationship between collagen and the apatic crystallites, in *Ultrastructure of Skeletal Tissues* (Kluwer Academic Publisher, 1990), pp. 41–62.
23. E. Mosler, W. Folkhard, E. Knorzer, J. Mol. Biol. **182**, 589 (1985).
24. W. Folkhard, E. Mosler, W. Geercken, E. Knorzer, H. Nemetscheck-Gansler, Th. Nemetscheck, H.J. Koch, Int. J. Biol. Macromol. **9**, 169 (1987).
25. M. Comminou, I. Yannas, J. Biomech. **9**, 427 (1976).
26. M. Maes, V. Vanhuyse, W. Decraemer, E. Raman, J. Biomech. **22**, 1203 (1989).
27. T. Gottesman, Z. Hashin, J. Biomech. **13**, 89 (1980).
28. A. Hodge, J. Petruska, *Electron microscopy* (Academic Press, New York, 1962).
29. J.L. Katz, K. Ukraincik, J. Biomech. **4**, 221 (1971).
30. J.L. Katz, *The structure and biomechanics of bone. Mechanical Properties of Biological Materials'* (Cambridge University Press, Cambridge, 1979), Vol. 34, pp. 137–168.
31. Y. Lanir, J. Biomech. **16**, 1 (1983).
32. J. Humphrey, F. Yin, J. Biophys. **52**, 563 (1987).
33. J.D. Currey, Clin. Orthopead. Related Res. J. **73**, 210 (1970).
34. R.S. Gilmore, J.L. Katz, J. Mater. Sci. **17**, 1131 (1982).
35. A. Ascenzi, E. Bonucci, Anat. Record J. **158**, 375 (1967).
36. D.T. Reilly, A.H. Burstein, J. Biomech. **8**, 393 (1975).
37. M. Pithioux, Lois de comportement et modèles de rupture des os longs, University Aix Marseille II, thesis 2000.
38. H. Liao, S.A. Belkoff, J. Biomech. **32**, 183 (1999).
39. C. Hurschler, B. Loitz-Ramage, R. Vanderby, J. Biomech. Eng. **119**, 392 (1997).